Research Article

Photocatalytic activity of biosynthesized CeO$_2$ nano particles

G. Ramanathan[1] · S. Vinoth Rathan[1] · K. R. Murali[2]

Abstract

This paper focuses on a cost effective and environment friendly technique for green synthesis of cerium oxide (CeO$_2$) nano particles from cerium (III) nitrate hexahydrate solution by co-precipitation method using the leaf extract of different species of Artemisia pallens which acts as reducing and capping agent. The prepared CeO$_2$ nano particles were characterized by XRD, TEM, FTIR, UV–Vis spectroscopy. The Photocatalytic activity of the prepared ceria powders was determined by their ability to degrade Methylene blue solution under UV-light radiation. The photo degradation result observed with 10 mg/L ceria at pH = 11 for 180 min have highest output and pseudo 1st order rate constant was 0.983.

Keywords Cerium oxide · Nanoparticles · Photocatalysis · Electronic material

1 Introduction

Nanotechnology is an emerging field of physics, chemistry, biology, engineering and electronic application. It involves the creation and/or manipulation of materials at the nano meter scale which contains single groups of atoms or bulk materials. Nano dimension of a material induces significant change of its properties namely optical absorption, electrical conductivity, chemical reactivity, biocompatibility compared to the macro dimension of the materials. With reduction in particle size, the surface area increases outstandingly and the number of atoms situated on the surface of the particles is higher which grants a considerable change of morphology properties [1]. Generally nano particles have large surface to volume ratio when compared to their bulk form. In general, large numbers of surface atoms are present compared to bulk materials, which play a vital role in an energetic state making significant contribution to the total free energy. These factors can change the properties such as reactivity, mechanical strength and electrical characteristics. Presently nano particles are widely used in technological application like LEDs, sensors and solar cell etc. [2–4]. Semiconductor nano particicels

usually exhibit variable as well as often controllable properties. In general when the size of the particle decreases, there is a change of energy structure and hence enhances surface properties. This will enhances their optoelectronic properties. Cerium is a rare earth element, which exists in trivalent state; cerium also occurs in IV states and may alternate between these two in a redox reaction. Based on this results, it was theorized that cerium oxide nano particles prolong cellular longevity by scavenging free radicals generated during their lifetime. The distinct structure of ceria nano particles with regard to the valence, support cell longevity which is a benefit of its antioxidant properties. Antioxidant behaviour is strongly influenced by the co-existence of both Ce3+ and Ce4+ oxidation states in CeO$_2$ nano particles. Cerium di oxide has wide band gap (3.18 eV) energy. It is a technological important material, which has wider application such as super capacitor, buffer layers in conductors, fuel cell battery, polishing material, UV blockers and optical storage devices. It is an important material that can be used in photo catalytic reaction [5–10]. Several methods have been engaged to prepare ceria powder [11–16] were employed on the past decade. This paper focuses on preparing ceria nano powder using

✉ K. R. Murali, muraliramkrish@gmail.com | [1]Department of Physics, Sri Sairam Engineering College, Chennai 600 044, India. [2]Department of Theoretical Physics, University of Madras, Chennai, India.

green synthesis method. Many bioactive compounds are contained in Atemesia. It is known for its antimalarial activity and cytotoxicity against tumor cells [17]. These plants are also popular for the treatment of diseases such as hepatitis, cancer, inflammation and infections by fungi, bacteria and viruses [18]. It appears as a small and aromatic herbaceous plant and is native to the southern part of India. The leaves and flowers of this plant are highly valued for making floral decorations and oils. The plant consists of very small leaves, bluish green with yellow flowers. Traditional Ayurvedic medicinal formulations utilize this plant. The synthesized nano powder was characterized by x-ray powder diffraction,TEM and FTIR spectrum to study the structure and bonding nature. These samples were also studied for their photo catalytic activity using MB under UV light.

2 Experimental

The bio synthesis of ceria (CeO_2) nano particles were done by green chemistry method using cerium (III) nitrate hexahydrate. In the first step of synthesis 5 g of cerium (III) nitrate hexahydrate was added to 25 ml distilled water and stirred thoroughly at 60 °C for 1 h to form a clear solution. In the second step 10 g of Artemisia pallens was added into 50 ml distilled water and heated at 60 °C for 1 h. This solution was filtered and this filtrates was taken in a burette. This clear solution in burette was added as drop by drop to cerium (III) nitrate hexahydrate solution under constant stirring condition to form a precursor. In the third step, two tablets of NaOH were dissolved in 50 ml of distilled water and then added drop by drop into a beaker containing the precursors. A small quantity of NaOH was used to increase the pH to alkaline condition. After few hours precipitation occurred. This precipitate was centrifuged at 6000 rpm and was then dried at 373 K. The X-Ray diffraction patterns of the CeO_2 nano particles was recorded using panalytical's X-Ray diffractometer for various calcined temperatures. The FTIR spectrums of the CeO_2 nano particles were taken using Perkin Elmer spectrometer. The surface morphology and particle size of the CeO_2 nano powder were analyzed by Transmission electron microscopy (TEM) images were obtained with JEOL JEM 2010HR operating at 200 kV. Absorption spectrums for the CeO_2 nano particles were recorded by using Shimadasu UV visible spectrophotometer. The CeO_2 nano particles calcined at different temperature in the range of 400–500 °C were employed to study the degradation of Methylene blue dye under UV radiation from a 12 W UV lamp. Five centimeter distance was maintained between the photoreaction vessel and the lamp source. About 5 mg of CeO_2 photo catalyst was added to 10 mg/L of methylene

blue solution (100 ml) in a typical run. At regular intervals of 60 min, 3 ml of the above solution was centrifuged to separate the photo catalyst particles, The concentration of methylene blue in this solution was evaluated from the absorption spectrum obtained with the help of Hitachi UV–VIS–NIR spectrophotometer.

3 Result and discussion

X-Ray diffraction pattern of cerium oxide nano particles obtained in the range of 28° to 95° is shown in Fig. 1. XRD exhibits the following peaks (111), (220), (311), (400), (331), (422) and (511) corresponding to single phase cubic structure (JCPDS NO: 431002). The broad peaks show the nano size crystallites. Crystallite size was calculated using $2\theta = 28°48'$ (111) peak with the Scherrer formula

$$D = 0.9\lambda/\beta\cos\theta \qquad (1)$$

where λ is the wavelength of X-Ray, θ is the Bragg diffraction angle and β is the full width half maximum (FWHM) of the XRD peak appearing at the diffraction angle θ. The average crystalline size and dislocation density are tabulated in Table 1. Generally size of nanoparticles increases with increase of temperature due to the aggregation of individual particles. In this case as the calcinations temperature increases recrystallization takes place along with grain aggregation and hence an increase in grain size.

Figure 2 Shows the Infrared spectrum of raw CeO_2 powder and various calcinations temperature of the samples. FTIR spectrophotometer between 450 and 4000 cm^{-1}. FTIR studies have been used to confirm the formation of metal
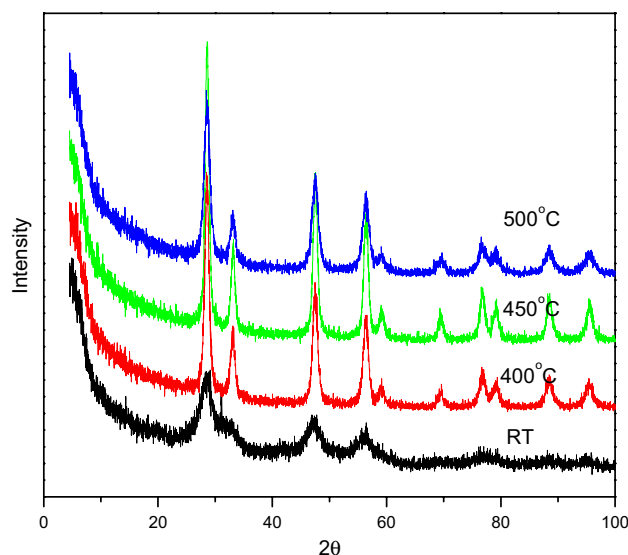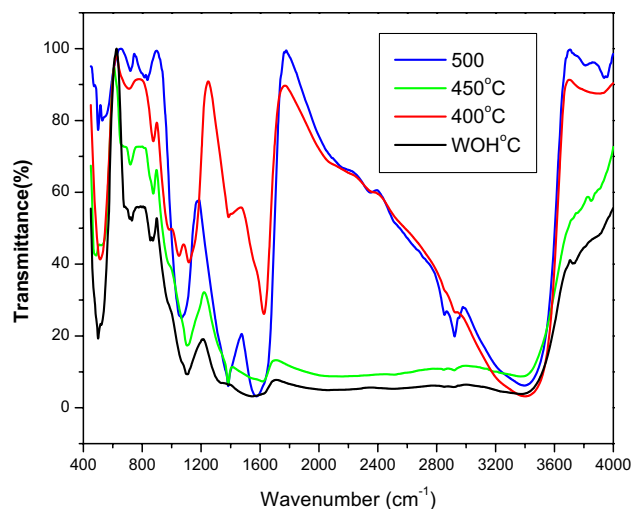

Fig. 1 XRD pattern of cerium oxide nano particle at different temperature **a** WHO, **b** 400 °C, **c** 450 °C, **d** 500 °C

Table 1 Grain size and dislocation density of CeO_2 nanopowders calcined at different temperatures

Temperature	Grain size (nm)	Dislocation density (10^{15})
WHO	3.612	76.6
400	10.29	9.44
450	12.10	6.88
500	13.35	5.61

Fig. 3 TEM image of CeO_2 nano particles prepared at different temperature. **a** 400 °C, **b** 450 °C, **c** 500 °C

oxide. The bands at 528 cm^{-1} and 719 cm^{-1} are due to the Ce–O stretching vibration whereas the bands at 1379 cm^{-1} and 1383 cm^{-1} are due to C-O stretching vibration and the band at 3395 cm^{-1} is due to O–H vibration of water absorbed from the moisture respectively [16].

Ultrafine nanoparticles of CeO_2 with average particle size in the range of 4.0 nm to 16.0 nm is observed in the TEM images (Fig. 3a, b) for the nanoparticles calcined at different temperature, Nearly spherical particles are observed. Thos results agrees well with the aize calculated using Scherrrer's equation from XRD data. A fairly uniform distribution of particles is observed. The average fringe distance between two adjacent fringes in the HRTEM pattern (Fig. 3c) is 0.31 nm. The selected area diffraction (SAED) pattern of the CeO_2 nanoparticles calcined at 450 °C (Fig. 3d) indicates the mulilayered pattern of the particles which is suggestive of a polycrystalline nature of

the particles as is supported by the mixed fringes pattern observed in HRTEM result.

The EDS spectrum shows the presence of Ce and O element no other element were observed in this spectrum (Fig. 4). Figure 5 shows the transmission spectra of prepared CeO_2 nano particles in the range of 100–1000 nm. The energy band gap of CeO_2 materials were calculated

Fig. 2 The FTIR spectra of cerium oxide nano particles prepared at different temperature WOH-without heat treatment
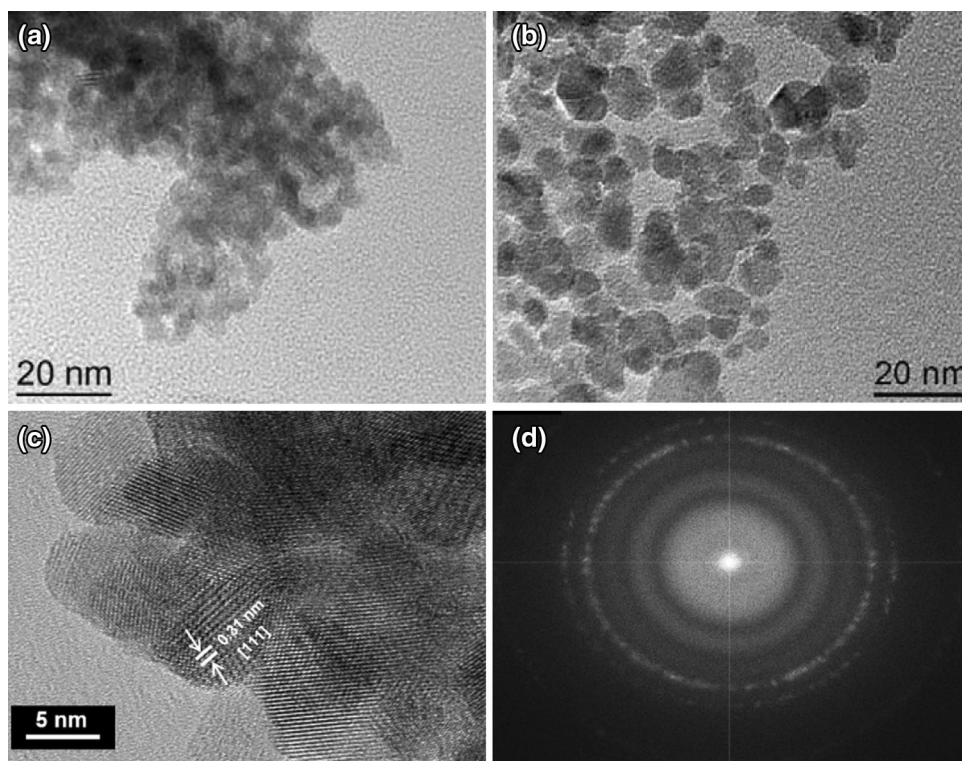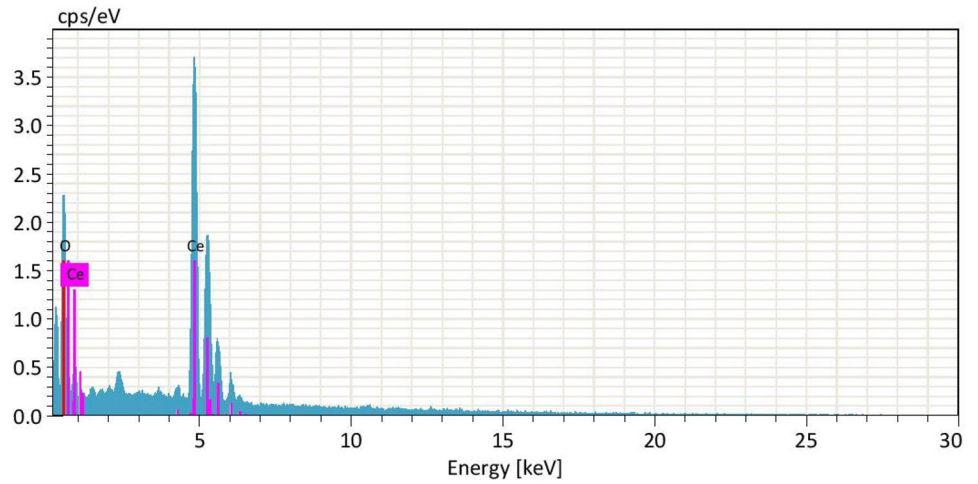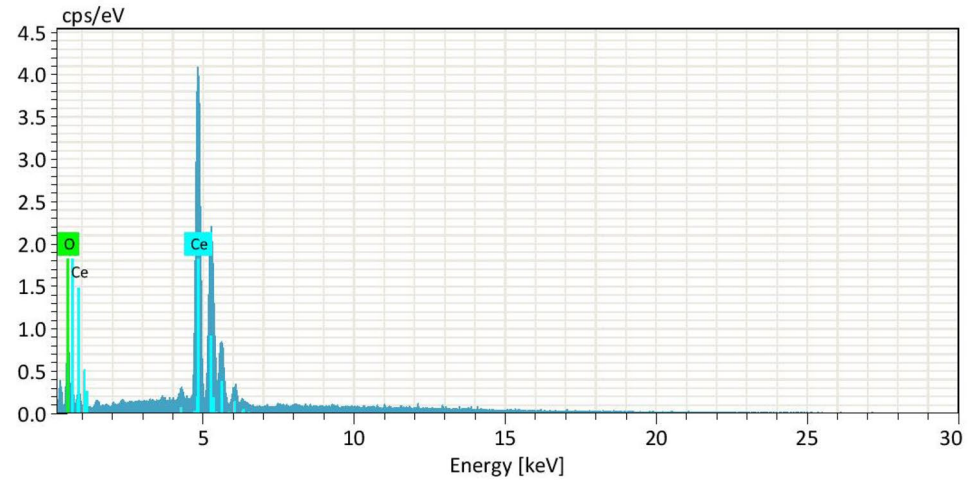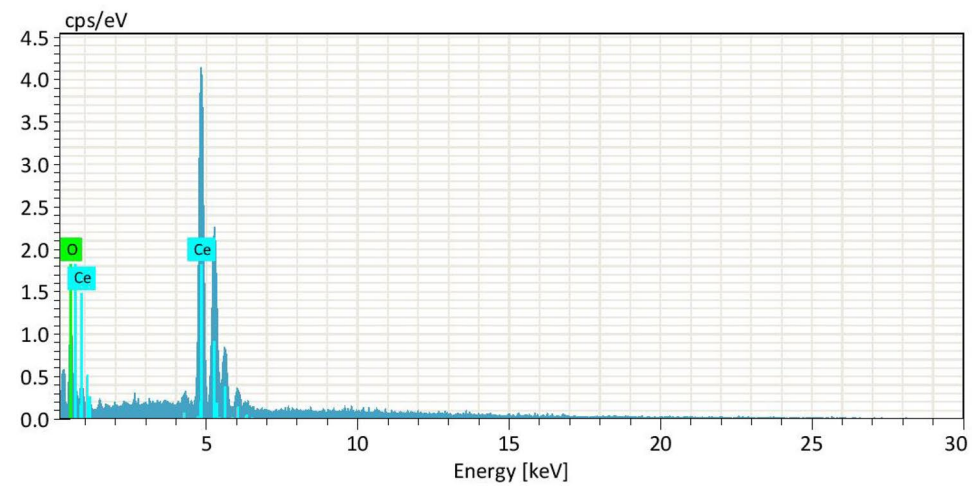
Fig. 4 EDAX spectrum of different temperature **a** without heat treatment (WOH), **b** 450 °C, **c** 500 °C

(a) Without calcination

(b) Calcined at 250°C
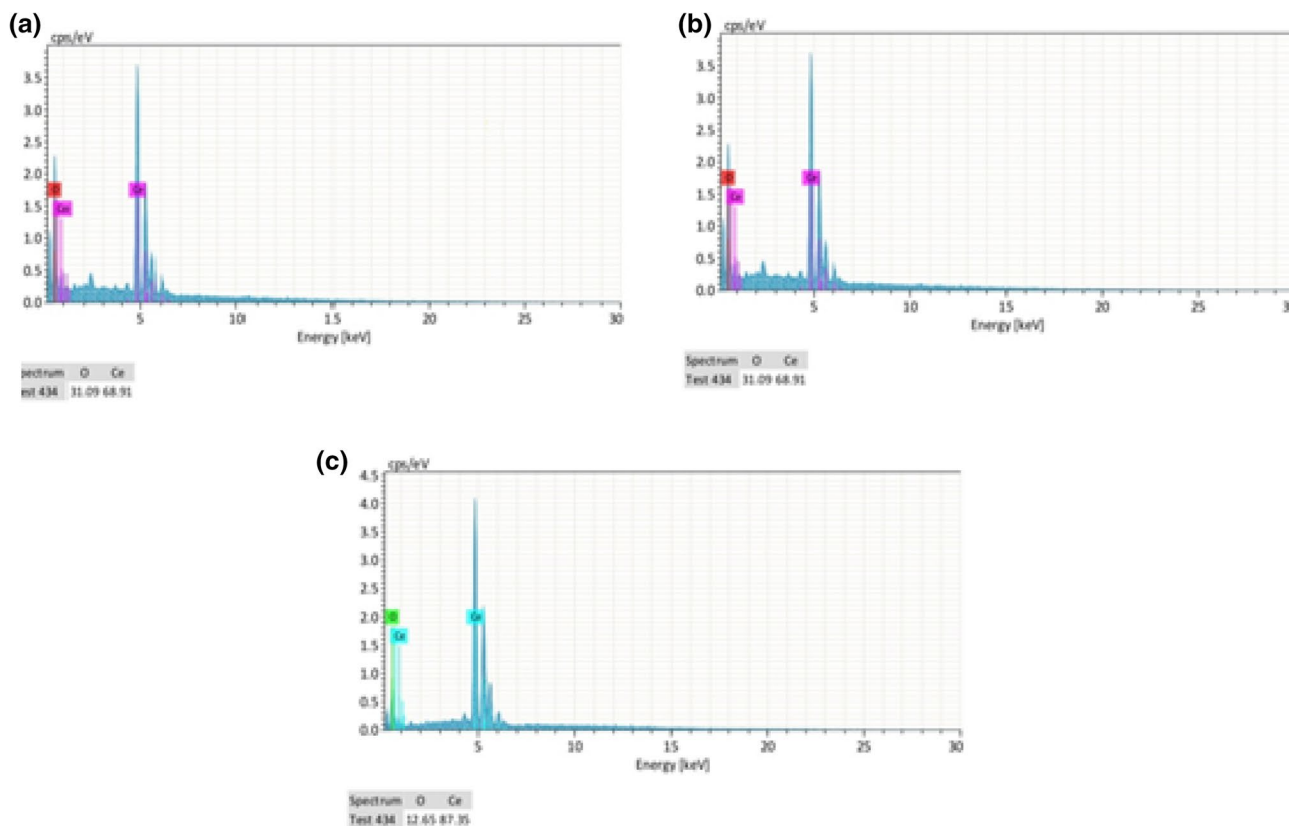

(c) Calcined at 450°C

Fig. 5 UV–Visible transmission spectra of cerium oxide nano particles at different temperature

using optical transmission spectrum. The formula is given by

$$E_{bg} = 1240/\lambda \, eV \qquad (2)$$

where λ is the wavelength (nm) and Ebg is the optical band gap energy. The optical band gap of CeO_2 is 3.45 eV that is quite large compared to reported value (3.22 eV) of bulk CeO_2 [19, 20]. The enhancement in optical band gap of CeO_2 nano particles could be due to the quantum size effect and it is consistent with literature report for CeO_2 nanoparticles [21].

3.1 Photocatalytic activity studies

In analytical chemistry MB is widely used as a redox indicator. MB is a dark green powder that yields a blue solution in water. In blue bottle experiment, MB is an oxidizing environment and turn colourless when exposed to a reducing agent. In biological field, MB is used to examine RNA or DNA under a microscope or in a gel. Photocatalytic activities of the CeO_2 nano particles was studied by decolourization of methylene blue (MB) aqueous solution under stimulated UV radiation.

3.2 Degradation of MB catalysed by cerium oxide

The degradation efficiency of MB (10 mg/L) versus time in the absence and presence of CeO_2 nanoparticle (10 mg/L) at a pH of 11 are shown in Fig. 6 In the absence of any photocatalyst the degradation of the MB molecule occurs under UV irradiation at a slow rate. This degradation efficiency with irradiation increases in the presence CeO_2
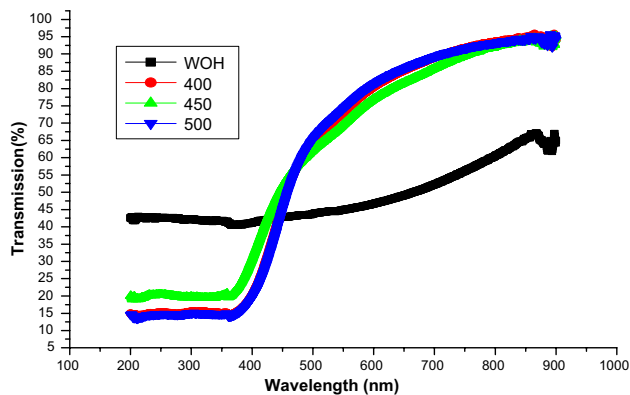

Fig. 6 Degradation efficiency with time of MB (10 mg/L) at pH11 catalyzed by CeO_2 nanoparticle calcined at different temperature

nano particles, since the onset of absorption is lower than 420 nm wavelength which is suitable for transfer of electron from the valence band to conduction band [22]). This leads to formation of holes and electrons in the valence band and conduction band respectively. The holes in valance band react with water which leads to degradation of the dye by the interaction of holes and OH species. [23] The highest photocatalytic activity is observed for the samples calcined at 500 °C. Photo catalytic activity is affected by particles size, crystallinity and surface properties. Preparation method can control the above factor along with the catalytic loading. Nanomaterials have unique adsorption properties in addition to high specific surface area and its disordered surface region [24]. Though the as synthesized and powders calcined at temperatures below 500 °C possess high surface area compared to the powder calcined at 500 °C, the highest photocatalytic activity of the high temperature calcined powder can be explained as a result of the improved crystallinity of these powders. The degradation efficiency of MB (10 mg/L) at different photocatalyst dosages ranging from (5 to 40 mg/L) at pH 11 have been studied. Figure 7 shows the photodegradation efficiency of MB which increases as the amount of photocatalyst was increased up to 5 mg/L and thereafter decreases with increase in photocatalyst loading. The availability of actives sites and thus an increase in the number of dye molecule adsorbed on the surface of the catalyst as well as an increase in the density of particle in the illumination area is the reason for the increase in decolourization rate [25, 26]. At the higher catalyst loading of 40 mg/L, the dye degradation rate decreases due to agglomeration of the photocatalyst. This results in decrease of the radiation penetration depth and causes radiation scattering at higher

photo catalyst concentrations. Therefore it is desirable to add the optimum amount of CeO_2 to avoid the presence of excess catalyst and thus ensure the total absorption of light photons for efficient photodegradation.

The pH of the dye plays an important role in dye degradation, since, the adsorption capacity of dyes on the photo catalyst is an important factor. An increase in the rate of molecule decomposition is the result of an increase in the number of target molecules adsorbed onto a catalyst [27]. In this study, the effect of pH on the photocatalytic activity of CeO_2 nano particles (10 mg/L) during the MB degradation process with an initial concentration of 5 mg/L over a pH ranges 1–12 was studied. The pH of the dye solution was adjusted by adding suitable amounts of HCL for pH range up to 6, beyond which NaOH (concentrations of 10 mg/L). The degradation yield in the different pH solution is shown in Fig. 8. The results show that the maximum degradation efficiency was observed at a pH of 11. This is due to the fact that, higher the pH of the solution, the higher will be the concentration of hydroxyl ions for reaction with the holes and for the formation of hydroxyl radicals. Due to the negative charge of the catalyst surface, adsorption of positively charged dye molecules occurred in the basic solution. Inhibition of dye degradation occurs at a pH higher than 11, since, under these conditions, the hydroxyl ions compete with dye molecules in the adsorption on the catalysts surface [28, 29]. Figure 9 shows the effect of initial concentration of MB dye (5–40 mg/L) on the rate of degradation of the dye. A decrease in the rate of degradation is observed for an increase in the initial MB concentration. There are two factors, that are responsible for the decrease in degradation efficiency with an increase in the initial dye concentration, viz., an increase in the number of dye molecules adsorbed on the surface of the catalyst leads to a decrease in the number of active sites that generate hydroxyl radicals, and an increases in the light absorbed by the dye molecules leads to a decrease in the number of photons that reach the catalyst surface [30].

The influence of many factors and their mutual effects heterogeneous photocatalysis reactions are complicated processes. In this study, MB photo degradation followed a pseudo first order kinetic expression as shown in Fig. 10). Langmuir–Hinshelwood kinetic expression is followed in this study similar to earlier reports [31].
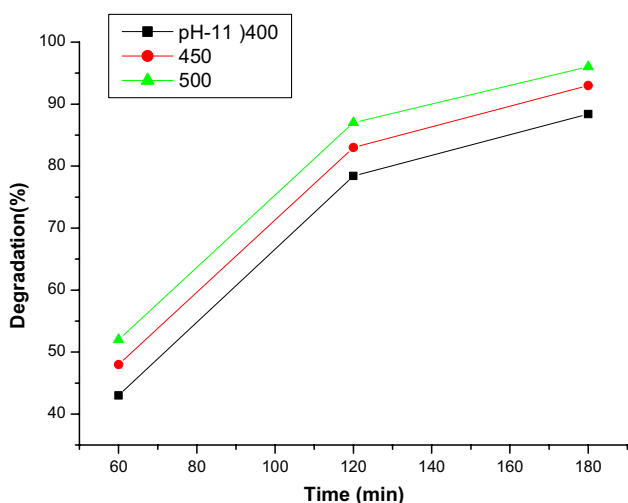
$$r = d[dye]/dt = kk_{dye[dye]}/(1 + k_{dye}[dye]_0) = K_{dye}[dye] \tag{3}$$

$$1/k_{app} = (1/kk_{dye}) + \{[dye]_0/k\} \tag{4}$$

In Eqs. 3 and 4, [dye]o is the initial concentration of MB (mg/L), kdye is the Langmuir–Hinshelwood adsorption equilibrium constant (L/mg),k is the rate constant of the
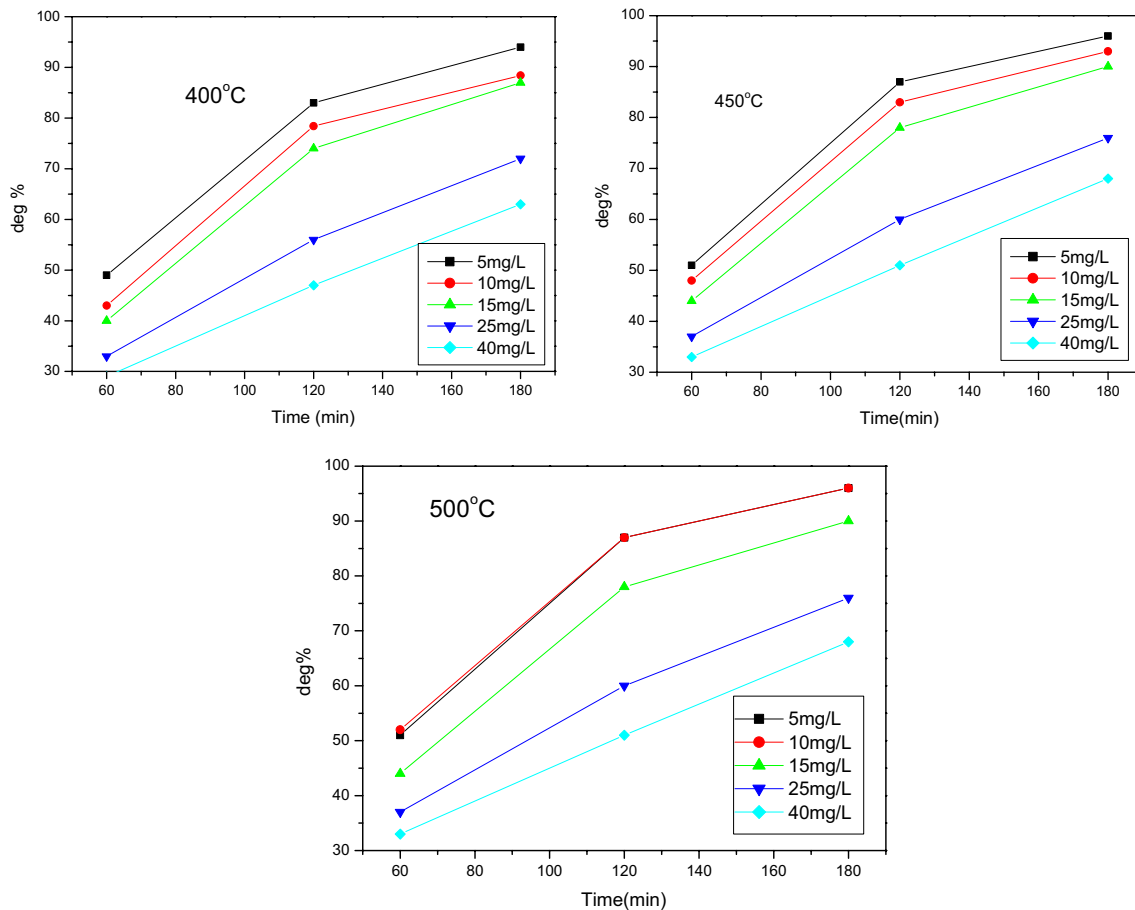

Fig. 7 Degradation efficiency of MB (10 mg/L) catalyzed by nanoparticles at different photocatalyst loading at pH11

Fig. 8 Degradation efficiency of MB (10 mg/L) catalyzed by CeO_2 nanoparticle at different pH values

surface reaction (mg/L min) and k_{app} is the pseudo first order rate constant. According to Eq. 4, a plot of $1/k_{app}$ versus [dye] is a straight line and in this case the rate constant for the surface reaction is k = 0.188 mg/(L min) and the adsorption equilibrium constant k_{dye} = 0.102 for the powder calcined at 500 °C (Fig. 10). The obtained regression coefficient R is 0.983, which suggests that the photo degradation of MB catalyzed by CeO_2 fits the Langmuir–Hinshelwood kinetic model, and also leads to the conclusion that the CeO_2 powders calcined at different temperature in the present work can be an efficient photocatalyst for the degradation of Methylene blue (Table 2).

Photocatalytic degradation of an organic dye can be understood as follows. As the first step, MB dye adsorbs onto the nano CeO_2 surface. When the CeO_2 is irradiated with UV light, electron- hole pairs are created. While the photo generated electrons in the conduction band of CeO_2 interact with the oxygen molecules adsorbed on the CeO_2 to form the superoxide anion radicals (O_2^-), the holes generated in the valence band of CeO_2 react with the surface nydroxyl groups to form highly reactive hydroxyl radicals ($OH^.$). These two highly reactive radicals react with the MB dye adsorbed on

the photocatalysrt resulting in the decolouration and hence degradation of the dye [32, 33]. The two important factors for a good catalyst to be used in practical applications are its recyclability and stability [34]. The degradation/regeneration capacity and hence the structural stability during the entire process was evaluated by studying the reusability of the photocatalyst for 5 cycles. Initially the rate of decrease of the degradation efficiency is fast and after the 4th cycle, the rate of decrase is slow compared to the first three cycles. There is 5% decline in the degradation efficiency after 5 cycles (Fig. 11). This stands testimony to the excellent photocatalytic activity of the CeO_2 nanopowder synthesized in this work.

4 Conclusion

Ceria nano particle were prepared using cerium (III) nitrate hexahydrate and NaOH as precursors in the absence of any capping agent using the extract of Artemisia pallens. The photo generated holes are the major active species of Cerium oxide in the photo catalytic degradation of MB.
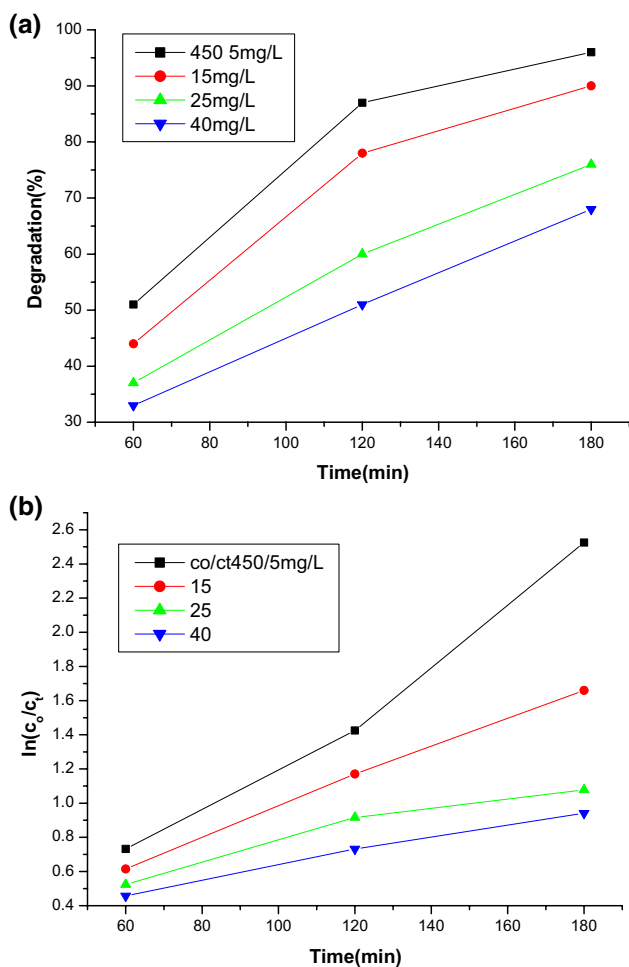
Fig. 9 Degradation efficiency (**a**) and Plot of In (co/ct) versus time (**b**) at different initial dye concentration (5–40 mg/L) catalyzed by CeO_2 nanoparticle (10 mg/L) at pH 11

The results revealed that the smaller size CeO_2 nanoparticles are potential photo catalyst for the degradation of methylene blue. The MB degradation shows the highest photocatalytic reactivity at pH 11 for CeO_2 calcinated at 500 °C. In the presence of OH and superoxide radicals considerable reduction is observed in the colour of MB. This shows that the photo generated holes and electrons in the catalyst upon irradiation plays an important role in photo degradation. The photocatalyst could be reused for 5 cycles with a decline of only 5% efficiency in the degree of degradation. The excellent reusability if the synthesized CeO_2 nano powders indicates the efficient utilization of these materials in environmental remediation.
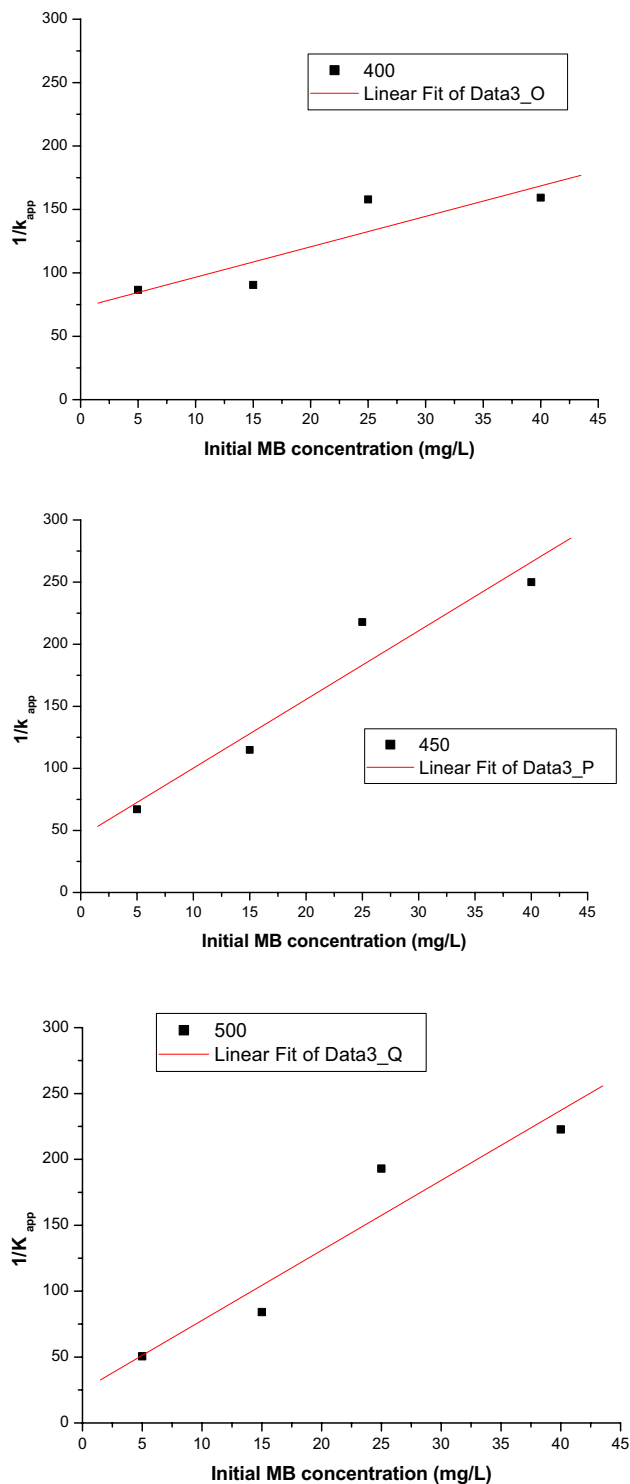

Fig. 10 Plot of $1/K_{app}$ versus initial concentration of MB for the CeO_2 photo catalysts sintered at different temperatures

Table 2 Rate constants and half lifetime of CeO$_2$ photocatalysts calcined at different temperatures

Temp	Dye conc. (mg/L)	K$_{app}$/min 10^{-3}	1/K$_{app}$	t$_{1/2}$/min	Regression coefficient R
400°C	5	11.56	86.50	59.95	0.875
	10	12.98	77.04	53.39	
	15	11.06	90.41	62.66	
	25	6.33	157.9	109.4	
	40	6.28	159.21	110.3	
450°C	5	14.93	66.97	46.42	0.965
	10	9.33	107.18	74.28	
	15	8.71	114.8	79.57	
	25	4.59	217.8	151.0	
	40	4.00	250	173.2	
500°C	5	19.79	50.53	35.02	0.95
	10	10.27	97.37	87.48	
	15	11.89	84.10	58.29	
	25	5.18	193	133.8	
	40	4.45	222.7	155.7	
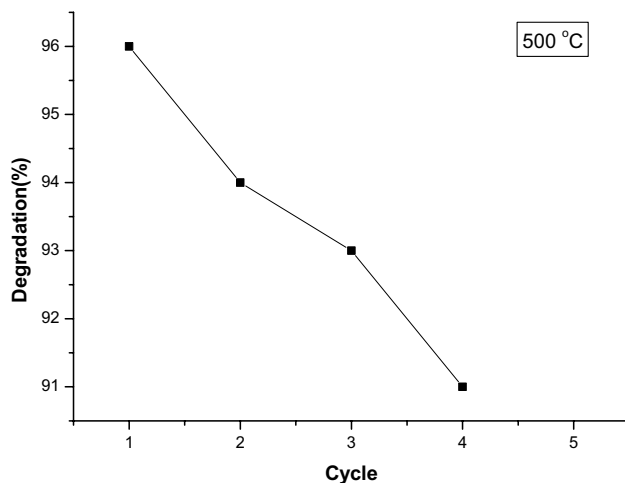
Fig. 11 Reusability of CeO$_2$ treated at 500 °C for the photodegradation of MB for 5 cycles

References

1. Pop OL, Diaconeasa Z, Mesaroş A, Vodnar DC, Cuibus L, Ciontea L, Socaciu C (2015) FT-IR studies of doped cerium oxide nanoparticles and natural zeolite. Mater Bull UASVM Food Sci Technol 72:50–55
2. Zhang Y, Andersson S, Muhammed M (1995) Synthesis of doped cerium oxides as oxygen storage promoters. Appl Chem B Environ 337:6325–6337
3. Lira-Cantu M, Norrman K, Andreasen JW, Krebs FC (2006) Oxygen release and exchange in niobium oxide MEHPPV hybrid solar cel. Chem Mater 18:5684–5690
4. Abecassis-Wolfovich M, Jothiramalingam R, Landau MV, Herskowitz M, Viswanathan B, Varadarajan TK (2005) Cerium incorporated ordered manganese oxide OMS-2 materials-improved catalysts for wet oxidation of phenol compounds. Appl Catal B Environ 59:91–98
5. Matijevic E, Hsu WP (1987) Preparation and properties of monodispersed colloidal particle of lanthanide compounds I Gadolinium europium terbium samarium CeO$_2$. J Colloid Interface Sci 118:506–510
6. Chen PL, Chen IW (1993) A theoretical model and experiments for the pop-out phenomena via Nanoindentation test of diamond films. J Am Ceram Soc 76:1577–1581
7. Li T, Ikegami JG, Wang YR, Mori T (2002) Synthesis of Graphene-scattered Nano Li$_2$Fe SiO$_4$ for lithium ion battery application. J Am Ceram Soc 85:2376–2382
8. Tsunekawa S, Sivamohan R, Ohsuna T, Kasuya A, Takasashi H, Tohji K (1999) Indirect exchange coupling of magnetic moments in Rare earth metals. Rare Earths 439:315–317
9. Djuricic B, Pickering S (1999) Nanocrystallization and phase transformation in monodispersed ultrafine Zirconia particle from various homogeneous precipitation method. J Eur Ceram Soc 19:1925–1932
10. Zhon XD, Hucbner W, Anderson HU (2002) Vaporization thermodynamics MgB$_2$ and MgB$_4$. Appl Phys Lett 80:2892–2894
11. Deluga GA, Salge JR, Schmidt LD, Verykios XE (2004) Renewable hydrogen from ethanol by autothermal reforming. Science 203:993–997
12. Hu J, Li Y, Zhou X, Cai M (2007) Preparation and characterization of Ceria nanoparticle using crystalline hydrate cerium propionate as precursor. Mater Lett 61:4989–4992
13. Wang H, Zhu JJ, Zhu JM, Liao XH, Zu S, Ding T, Chen HY (2002) Preparation of nano crystalline ceria particle by sono chemical and microwave assisted heating methods. Phys Chem Chem Phys 4:3794–3799
14. Shin G, Wang Q, Wang Z, Chen Y (2011) Full ALD Al$_2$O$_3$/ZrO$_2$/SiO$_2$/Al$_2$O$_3$ stacks for high performance MIM capacitors. Mater Lett 65:1211–1214
15. Ketzid JJ, Nesara AS (2011) Synthesis of CeO$_2$ nanoparticles by chemical precipitation and the effect of a surfactant on the distribution of particle size. J Ceramic Process Res 12(1):74–79
16. Prabaharan DM, Sadaiyandi K, Mahendran M, Sagadevan S (2016) Structural optical morphological and dielectric properties of cerium oxide nano particles. Mater Bull 19:478–482
17. Eckstein-Ludwig U, Webb RJ, Van Goethem ID, East JM, Lee AG, Kimura M (2003) Artemisinins target the SERCA of plasemodium falciparum. Nature 424:957–961
18. Cavaletti G, Bogliun G, Zincone A, Marzorati L, Melzi P, Frattola L, Marzola M, Bonazzi C, Cantù MG, Chiari S, Galli A (1998) Neuro and ototoxicity of high dose carboplatin treatment in poor prognosis ovarian cancer patients. Anticancer Res 18:3797–3802
19. Araujo VD, Avansi W, de Carvalho AH, Moreira ML, Longo E, Ribeiro C, Bernardi MI (2012) CeO$_2$ nano particle synthesized by a microwave assisted hydrothermal method evolution from nanospheres to nanorods. CrystEngComm 14:1150–1154
20. Phoka S, Laokul P, Swatsitang E, Promarak V, Seraphin S, Maensiri S (2009) Synthesis, structural and optical properties of CeO$_2$ nanoparticles synthesized by a simple polyvinyl pyrrolidone (PVP) solution route. Mater Chem Phys 115:423–428
21. Chen HI, Chang HY (2005) Synthesis of nanocrystalline cerium oxide particles by the precipitation method. Ceram Int 31:795–802
22. Brunaner S, Emmett PH, Jeller E (1938) Coordination compounds of palladous chloride. J AM Chem Soc 60:882–884
23. Culily BD (1978) Elements of X-ray diffraction reading. Addison Wesley, Boston
24. Hu CG, Zhang ZW, Liu H, Gao PX, Wang ZL (2006) Direct synthesis and structure of characteristics of ultrafine CeO$_2$ nanoparyicles. Nanotechnology 17:5983–5987

25. Xu J, Li G, Li L (2008) CeO_2 nanocrystals: seed-mediated synthesis and size control. Mater Res Bull 43:990–995

26. Height MJ, Pratsinis SE, Mekasuwandumrong O (2006) Praserthdam P Ag-ZnO catalysts for UV-photodegradation of methylene blue. Appl Catal B 63:305–312

27. Alkaim AF, Aljeboree AM, Alrazaq NA, Baqir SJ, Hussein FH, Lilo AJ (2014) Effect of pH on adsorption and photocatalytic degradation efficiency of different catalysts on removal of methylene blue. Asian J Chem 26:8444–8448

28. Ranjit KT, Willner I, Bossmann SH, Braun AM (2001) Photo degradation of organic pollutant using sol gel method. Environ Sci Technol 35:544–551

29. Pouretedal HR, Eskandrri H, Keshaverz MH, Semnani A (2009) Photodegradation of organic dyes using nanoparticle of cadmium sulphide doped with manganese, nickel and copper as nanophotocatalyst. J Acta Chem Solv 56:353–359

30. Pouretedal HR, Norozi A, Keshavarz MH, Semnani A (2009) Nanoparticles of zinc sulphide doped with manganese, nickel and copper as nano photocatalyst in the degradation of organic dyes. J Hazard Mater 162:674–681

31. Kumat PV, Meisel D (2002) Nano particle in advanced oxidation process. Curr Opin Colloid Interface Sci 7:282–290

32. Al-Ekabi H, Serpone N (1988) Kinetics studies in heterogeneous photo catalysis. J Phys Chem 92:5726–5731

33. Suna JH, Wang YK, Sun RX, Dong SY (2009) CeO_2 nanoparticle catalysis of methylene blue photodegradation: kinetics and mechanism. Mater Chem Phys 115:303

34. Li K, Yang C, Ying D, Wang Y, Jia J (2013) Effect of Inorganic anions on Rhoda mine β removal under visible light irradiation using BiO_2/Ti rotating disk reactor. J Chem Eng 211:208–213